Fission decay of ^{48}Cr at $E^*_{CN} \approx 60$ MeV

K. A. Farrar, S. J. Sanders, A. K. Dummer, A. T. Hasan, and F. W. Prosser
The University of Kansas, Department of Physics and Astronomy, Lawrence, Kansas 66045

B. B. Back, I. G. Bearden, R. R. Betts, M. P. Carpenter, B. Crowell, M. Freer,* D. J. Henderson, R. V. F. Janssens, T. L. Khoo, T. Lauritsen, Y. Liang, D. Nisius, and A. H. Wuosmaa
Argonne National Laboratory, Argonne, Illinois 60439

C. Beck and R. M. Freeman
Centre de Recherches Nucléaires, IN2P3-CNRS/Université Louis Pasteur, B.P. 28, F-67037 Strasbourg Cedex 2, France

Sl. Cavallaro
Dipartimento di fisica dell'Universitá di Catania, I-95129 Catania, Italy

A. Szanto de Toledo
Departamento de Física Nuclear, Instituto de Física da Universidade de São Paulo, Caixa Postal 20516-01498-970 São Paulo, S.P. Brazil

(Received 18 April 1996)

The fully energy-damped yields for the ^{36}Ar + ^{12}C and ^{20}Ne + ^{28}Si reactions at $E_{c.m.} = 47.0$ MeV and 45.5 MeV, respectively, are explored using particle-particle-γ coincidence data. These reactions reach a similar excitation energy of $E^*_{CN} = 59.5$ MeV in the ^{48}Cr compound nucleus as was obtained in an earlier particle-particle coincidence study of the ^{24}Mg + ^{24}Mg reaction. The overall mass and total kinetic energy distributions of the fission fragments are found to be well reproduced by statistical-model calculations. These calculations are also found to reproduce structure seen in the excitation-energy spectra for the ^{20}Ne + ^{28}Si and ^{24}Mg + ^{24}Mg exit channels for all three reactions. In previous excitation-function measurements, strong heavy-ion resonance behavior has been observed in elastic and inelastic cross sections for the ^{24}Mg + ^{24}Mg system. There has been speculation that peaks observed in the corresponding excitation-energy spectra at more negative Q values may also be a consequence of this resonance phenomenon. The observation of very similar behavior with the asymmetric-mass entrance channels makes it less likely, though, that the peaks arise from any special configuration of the compound system. Instead, an analysis of the γ-ray data and the results of statistical-model calculations support the conclusion that most of the observed high-lying structure can be accounted for in terms of statistical fission from a fully energy- and shape-equilibrated compound nucleus. For the ^{24}Mg + ^{24}Mg entrance channel, however, comparisons with the statistical model indicate a reduction of high-angular-momentum partial cross sections, leading to the ^{24}Mg + ^{24}Mg fission channel. For the first time, we are able to deduce the nature of the competition between the resonance and statistical-fission mechanisms in this mass region. [S0556-2813(96)03109-3]

PACS number(s): 25.70.Jj, 24.60.Dr, 25.70.Gh

I. INTRODUCTION

The systematics of fusion followed by fission in the mass $40 \leqslant A_{CN} \leqslant 80$ region have been well established (see Refs. [1,2], and references therein) and it is interesting to explore how this process competes with other mechanisms that result in binary yields. The ^{48}Cr nucleus provides a good system with which to explore such competition. The ^{24}Mg(^{24}Mg, ^{24}Mg)^{24}Mg reaction [3–5] is known to involve a resonance mechanism which has an important influence on yields at lower excitation energies ($\lesssim 8$ MeV). Although the correlations among the energy spectra for different mutual excitations are not as strong, the ^{20}Ne(^{28}Si, ^{24}Mg)^{24}Mg reaction [6] is also known to exhibit resonance behavior involving the low-lying states of ^{24}Mg. Furthermore, peaks are observed in excitation-energy spectra for the ^{24}Mg(^{24}Mg, ^{24}Mg)^{24}Mg reaction up to energies where secondary α-particle emission from the fragments starts to dominate the spectra, thereby obscuring any spectroscopic details. It is not clear if this peak structure has any relationship to the resonance behavior. Many of the observed peaks are, however, located at energies near to mutual excitations of members of the ^{24}Mg ground-state rotational band. It is believed that this band may play a special role in the resonance behavior as a consequence of its associated prolate deformation [5].

In order to examine the question of competition between the resonance and statistical fission processes, an earlier experiment was done [7] in which the compound ^{48}Cr* system was populated by way of the ^{24}Mg + ^{24}Mg entrance channel with $E_{c.m.} = 44.4$ MeV, corresponding to a ^{48}Cr* excitation energy of 59.4 MeV. In addition to cross sections and energy distributions for all of the major fission channels, high-

*Present address: School of Physics and Space Research, University of Birmingham, Birmington B15 2TT, England.

TABLE I. Summary of characteristic energies and angular momenta for the the three systems. The grazing angular momenta l_{gr} are based on optical model calculations for the respective channels. The critical angular momenta for fusion l_{cr} are based on the fission transition-state calculations. These values lead to the best reproduction of the observed fission yields. V_C is the calculated Coulomb barrier height.

System	E_{lab} (MeV)	$E_{c.m.}$ (MeV)	E^*_{CN} (MeV)	$E_{c.m.}/V_C$	l_{gr} ($\hbar$)	l_{cr} ($\hbar$)
^{36}Ar + ^{12}C	187.7	47.0	59.5	2.59	30.2	24.4
^{20}Ne + ^{28}Si	78.0	45.5	59.8	1.98	31.2	27.9
^{24}Mg + ^{24}Mg	88.8	44.4	59.4	1.89	30.5	30.4

resolution Q-value spectra were obtained for the ^{24}Mg + ^{24}Mg and ^{20}Ne + ^{28}Si exit channels. Each of these channels showed pronounced structure at high ($\gtrsim$10 MeV) excitation energy. Because of the large number of possible mutual excitations, with already about 30 per MeV at an excitation energy of 10 MeV for the ^{24}Mg + ^{24}Mg exit channel, it was not possible with the data from that experiment to associate the observed peaks with unique channels in the final state. Moreover, an analysis based on the assumption of a statistical population of the fragment states was in good qualitative agreement with the data.

In this paper we report on measurements of fissionlike yields where the ^{48}Cr system is populated using the asymmetric-mass ^{36}Ar + ^{12}C and ^{20}Ne + ^{28}Si reactions. A comparison of these results with those from the symmetric entrance channel and with the predictions of a statistical-model calculation is presented. These results illustrate the important role of statistical fission in the general behavior of this system, as well as its role in the population of levels in symmetric and near-symmetric decay channels. In particular, comparison of the mutual-excitation spectra shows that the existence of peaks at high energies is not specific to the entrance channel, but is characteristic of compound-nucleus decay. The γ-ray information obtained in these measurements also supports the conclusion, suggested by the model calculations, that much of the yield in these peaks can be understood in terms of a statistical population of the energy levels in the fragments where high-spin levels are favored.

Some of the characteristic energies and angular momenta for the ^{36}Ar + ^{12}C and ^{20}Ne + ^{28}Si systems are summarized in Table I. This table also includes the corresponding information for the earlier study of the ^{24}Mg + ^{24}Mg reaction [7].

Instead of calculating the compound-nucleus spin distribution leading to fission within a model space, it is possible to deduce this distribution based on the observed excitation-energy spectra by assuming a spin-weighted population of reaction fragments. The fission spin distribution can then be determined without knowledge of the fusion spin distribution and without calculation of the competition between light-particle evaporation and fission. Considering the ^{24}Mg + ^{24}Mg exit channel, for the ^{36}Ar + ^{12}C and ^{20}Ne + ^{28}Si entrance channels, the deduced centroids and widths of the corresponding fission spin distributions are consistent with those calculated with the statistical model. Comparable results for the ^{24}Mg + ^{24}Mg entrance channel, however, indicate an average spin value significantly lower than predicted by the model calculations. This suggests competition between the fission and heavy-ion resonance mechanisms and is the first direct evidence in this mass region that the heavy-ion resonance process influences the statistical properties of compound-nucleus decay.

The paper is organized as follows: In Sec. II the experimental arrangement is described and in Sec. III the experimental results are presented. In Sec. IV the statistical model used to describe the excitation-energy spectra is discussed and comparisons are made to the experimental results. It is also shown how the fission spin distributions can be deduced from the experimental spectra, based on the statistical-model calculations. Finally, Sec. V presents a summary of the principal results.

II. EXPERIMENTAL ARRANGEMENT

The ^{36}Ar + ^{12}C and ^{20}Ne + ^{28}Si measurements were carried out with beams from the ATLAS accelerator at Argonne National Laboratory using the Argonne-Notre Dame BGO γ-ray facility [8]. The experimental procedures employed for both entrance channels were similar to those described previously for a particle-particle-γ coincidence measurement of the ^{32}S + ^{24}Mg reaction [2].

For the ^{36}Ar + ^{12}C experiment, we used a 187.7 MeV ^{36}Ar beam incident on an isotopically enriched ^{12}C target of areal density 75μg/cm^2. Six Si[surface barrier (SB)] detectors were located at nominal laboratory angles of 16°, 8°, 4°, $-4°$, $-6°$, and $-10°$, with the sense of the angles as indicated in Fig. 1. Unit mass resolution was obtained with these detectors up to $A=36$ using the time structure of the ATLAS beam for time-of-flight measurement. The Si(SB) detectors were used to obtain cross section normalizations, to determine the fission and evaporation-residue energy and angular distributions, and to determine the angular offset of the beam through the chamber ($\simeq$0.1°). A Bragg curve spectrometer (BCS) [9] was located at an angle of 21° relative to the beam and at a distance of 111.7 cm from the target. This detector was used to determine the Z and energy of fission fragments at large angles, yielding better than unit nuclear charge resolution [see Fig. 2(a)] and $\simeq$ 1% energy resolution. Scattering yields off ^{197}Au targets were used for energy calibrations in the Si(SB) detectors and the Bragg curve spectrometer. Additional energy calibration information was obtained with an ^{241}Am α-particle source.

Two 20 cm $\times$ 20 cm active-area, position-sensitive, parallel-grid avalanche counters (PGAC's) [10] were used for the particle-particle coincidence measurement. A determination by these counters of the positions and relative time of arrival of the two fragments from binary events is sufficient for an event-by-event determination the fragment masses [see Fig. 2(b)] and the reaction Q values. These de-

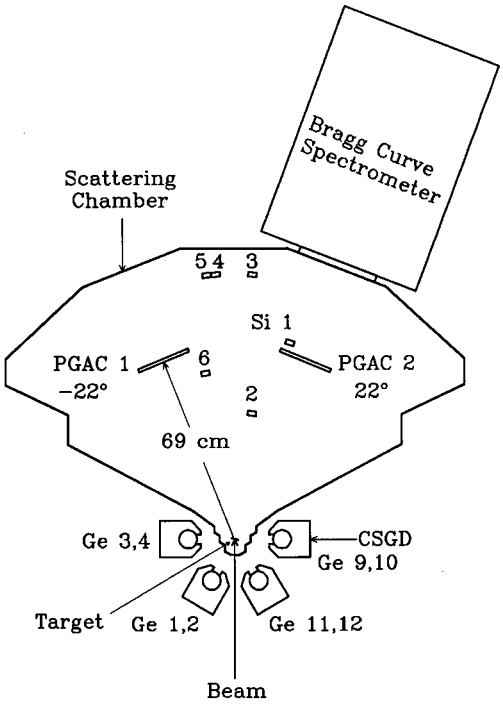

FIG. 1. Scale drawing of the scattering chamber showing the arrangement of particle and γ-ray detectors for the ^{36}Ar + ^{12}C experiment.

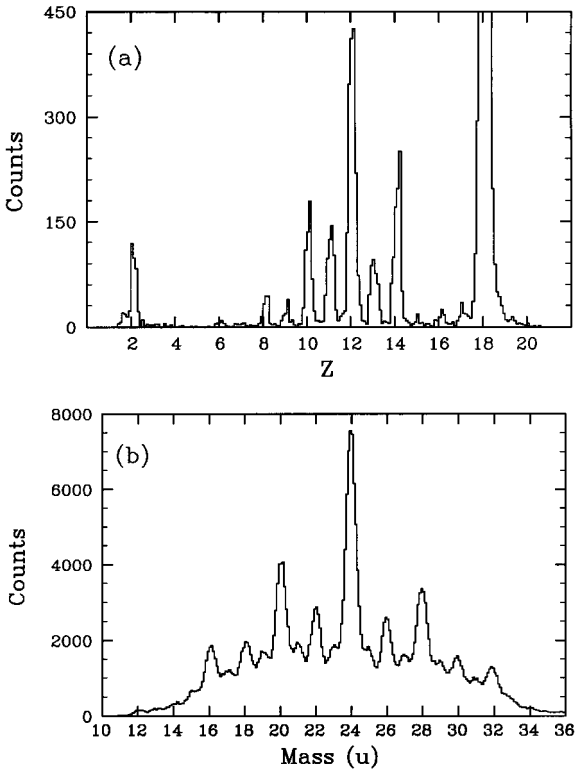

FIG. 2. (a) Typical Z spectrum obtained with data from one of four quadrants in the BCS. The yields observed at low values of Z were limited by the detection efficiency of PGAC2 which generated the trigger for the BCS. (b) Mass spectrum obtained from the coincidence measurement. The abscissa corresponds to the mass of the particle detected in PGAC1.

tectors were nominally positioned 69 cm from the target at $\pm 22°$ relative to the beam. PGAC2 was operated as a transmission counter backed by the BCS and Si1. The detection efficiency of the PGAC's, as a function of the mass of the detected particle, was determined with Si1 and by assuming reflection symmetry about the beam direction. The position and relative timing resolutions for these detectors were $\simeq 2$ mm and < 480 ps, respectively.

Data from the γ-ray array were taken in coincidence with the particle measurements. The complete array involves 12 Compton-suppressed Ge detectors (CSGD's). For the ^{36}Ar + ^{12}C and ^{20}Ne + ^{28}Si experiments, however, the forward four detectors were removed to allow room for a large scattering chamber. The remaining eight CSGD's were located 20° above and below the horizontal plane at angles of $\pm 90°$ and $\pm 145°$ to the nominal beam axis. The energy calibration was determined with ^{88}Y, ^{60}Co, and PuC [11] sources. The energy-dependent absolute efficiency calibration was obtained with ^{60}Co, ^{152}Eu, and PuC sources of known activities. Additional efficiency information was obtained by using ^{182}Ta and ^{56}Co sources for relative efficiency calibrations. For each calibration, the source was placed in the target position with the scattering chamber in place. The efficiency data were fitted with a four-parameter version of the equation suggested by McNelles and Campbell [12]. For energies above the 6.1 MeV line of PuC, this fit was used to extrapolate the efficiency calibration. The total efficiency for the eight Ge detectors falls off approximately exponentially from 0.39% at $E_\gamma = 1000$ keV to 0.10% at $E_\gamma = 5000$ keV and 0.040% at $E_\gamma = 15000$ keV.

The ^{20}Ne + ^{28}Si measurement was done with an experimental arrangement very similar to that used for ^{36}Ar + ^{12}C, with a 78.0 MeV ^{20}Ne beam incident on a ^{28}Si target of areal density 8μg/cm^2 backed by a 10μg/cm^2 carbon foil. In the coincidence measurement, contaminant reactions with the C backing could be separated from reactions with the ^{28}Si target through differences in the respective two-body kinematics. Again, energy calibrations in the Si(SB) detectors and the BCS were achieved by measuring scattering yields off ^{197}Au targets and by use of an ^{241}Am source.

The scattering chamber and γ-ray detector array combination used for the ^{20}Ne + ^{28}Si measurement was the same one used for the ^{36}Ar + ^{12}C measurement, although the placement of the particle detectors was different. Four Si(SB) detectors were located at nominal laboratory angles of $-7°$, $-13°$, $-19°$, and $-25°$. In addition, four Si(SB) detectors were nominally located at $\pm 4°$ and 4° above and below the beam. This arrangement was used to help in determining the angle offset of the beam through the chamber ($\simeq 0.4°$). The BCS was located at $-42°$ at a distance of 116.8 cm from the target. The two PGAC's were positioned 79 cm from the target at $\pm 47°$ relative to the beam. In this case PGAC1, located in front of the BCS, was operated in a transmission mode. The position resolution obtained in the PGAC's was somewhat better (< 1.5 mm) than was achieved in the ^{36}Ar + ^{12}C measurement, leading to better than unit mass resolution.

III. EXPERIMENTAL RESULTS

It is usually a good assumption for heavy-ion reactions to take the total fusion cross section as being the sum of the

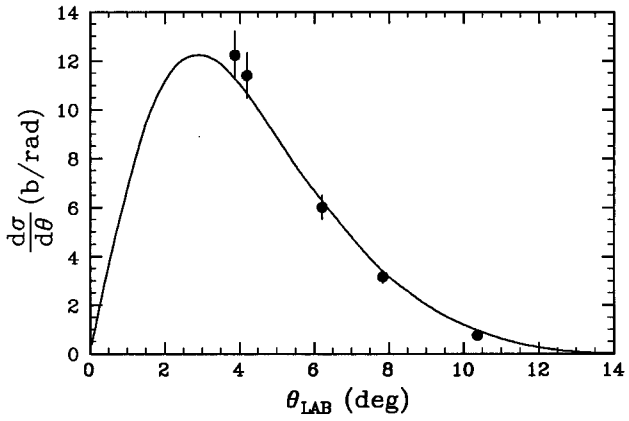

FIG. 3. Evaporation-residue angular distribution for the ^{36}Ar + ^{12}C reaction. The error bars show the statistical uncertainty associated with the data points. The solid line represents a distribution calculated with the program PACE scaled to the cross sections deduced from the experimental data.

evaporation-residue σ_{ER} and fission σ_{fis} cross sections. In heavier systems these two processes involve well-separated mass distributions and are therefore easy to distinguish experimentally. For lighter systems, where the fission process favors the mass-asymmetric breakup of the compound system, there is no clear demarcation between the masses associated with the two processes, although it is common to take ''fission'' as being associated with decay to masses greater than that of the alpha particle. In attempting to model the compound-nucleus decay to evaporation-residue and fission channels, knowledge of the total fusion cross section is useful by helping to constrain the normalization of the compound-nucleus spin distribution.

In this section, measurements of the evaporation-residue and mass-dependent fission cross sections for the ^{36}Ar + ^{12}C reaction are first presented. Similar results were not obtained for the ^{20}Ne + ^{28}Si measurement since reactions off of the carbon target backing and artifacts in the identification spectra resulting from slit scattering prevented a reliable extraction of singles yields. The particle-particle coincidence data, which allowed for high-resolution excitation spectra to be obtained for the near-symmetric-mass breakup of both incident channels, are then presented, followed by a discussion where the additional γ-ray data are used to help understand the nature of the peaks observed in these spectra.

A. Evaporation residue measurement

For the ^{36}Ar + ^{12}C reaction, the total evaporation-residue cross section σ_{ER} was obtained with singles measurements using the Si(SB) detectors. The program PACE [13] was used to calculate the evaporation-residue angular distribution $d\sigma/d\theta$ for $A \geq 38$, adjusting the value of the fusion critical angular momentum l_{cr} to achieve the best agreement with the corresponding experimental distribution. This mass region is expected to be relatively free of fission yields. The PACE results were used to extrapolate the $A \geq 38$, evaporation-residue $d\sigma/d\theta$ values observed at each angle to their corresponding mass-inclusive values. The resulting values of $d\sigma/d\theta$ and a curve representing the PACE distribution are shown in Fig. 3. The magnitude of the extrapolation ranged from 7% of the measured value for the 4° Si(SB) detectors to 37% for the 10° Si(SB) detector. Based on the fission calculation presented in Sec. IV, the *total* fission cross section for $4 < A_{fragment} \leq 10$ is estimated to be < 21 mb. If this is distributed with $d\sigma/d\theta$ = const, as expected for the binary decay of a long-lived, high-spin system, then we obtain $d\sigma/d\theta \leq 6.7$ mb/rad. For $44 > A \geq 38$, σ_{ER} was calculated with PACE to be 850 mb.

The PACE distribution was integrated to obtain $\sigma_{ER} = 1215 \pm 67 \pm 174$ mb. The first quoted uncertainty is the standard deviation of the PACE distribution from the experimental values, and the second is an estimate of the uncertainty associated with extrapolating $d\sigma/d\theta$ outside of the experimental angular range. This second uncertainty was taken as $\Delta\sigma_{ER} = \sigma(\theta_{lab} > 10.4°) + 0.25\sigma(\theta_{lab} < 3.9°)$.

B. Fission singles measurement

Cross sections were determined for the dominant ^{36}Ar+ ^{12}C fission decay channels from $A = 6$ to $A = 24$, with the exception of the ^{8}Be channel, using data from the Si(SB) detectors at 8°, −10°, and 16°. Since ^{8}Be is α-particle unbound, it could not be identified in this measurement. Because of low counting statistics, yields for mass channels in the range $A = 13$–15 were combined. For the $A = 20$ and $A = 24$ channels, the range of angular coverage was extended with $Z = 10$ and $Z = 12$ data from the BCS. The yields in these channels are dominated by ^{20}Ne and ^{24}Mg, as established by the simultaneous measurement of mass and charge for particles detected in the BCS and in coincidence with particles detected in PGAC1. This is in agreement with what has been observed in other light systems [14,7] and with the overall systematics of fission in these systems [1] where the $4n$, ''alpha-particle-like'' channels are found to be strongly populated. The average total kinetic energy $\langle E_{TKE} \rangle$ in the center-of-mass frame was calculated for each mass channel by using the centroid of the observed energy distribution and by assuming two-body kinematics.

For all decay channels of the ^{36}Ar + ^{12}C reaction, $d\sigma/d\theta$ and $\langle E_{TKE} \rangle$ were found to be independent of the center-of-mass angle in the range measured, corresponding to decay from a fully energy-damped, long-lived intermediate complex. Assuming $d\sigma/d\theta$ = const, the fission mass distribution shown in Fig. 4 is obtained. The measured $\langle E_{TKE} \rangle$ values are shown in Fig. 5.

C. Excitation-energy spectra

Experimental excitation-energy spectra for the ^{24}Mg + ^{24}Mg and ^{20}Ne + ^{28}Si exit channels were obtained for all three entrance channels using data from particle-particle coincidence measurements. In each case, Monte Carlo simulations were used to determine the coincidence efficiency of the respective experimental geometries, assuming $d\sigma/d\theta$ = const for the binary fragments. The efficiency-corrected $d\sigma/dE$ spectra are shown as thick-line histograms in Figs. 6 and 7. As a consistency check, a $d\sigma/dE$ spectrum was also obtained with the singles data from the BCS and PGAC2 for the ^{12}C(^{36}Ar, ^{24}Mg)^{24}Mg reaction, using the same code to extrapolate outside of the experimental angular acceptance as

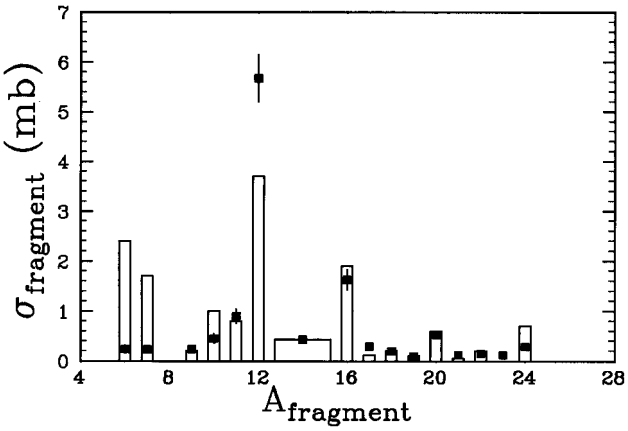

FIG. 4. Observed (solid symbols) and calculated (histogram) mass distributions for the fully energy-damped yields. Masses 13–15 are represented by their average cross section. The cross sections for mass 8 are not included since this channel was not experimentally accessible. When not shown, uncertainties are smaller than the symbol.

used for the coincidence efficiency calculation. The spectrum was integrated over all energies and the resulting ^{24}Mg cross section was found to be 0.30 ± 0.04 mb. This is in excellent agreement with the equivalent cross section deduced from the Si(SB) detector data of 0.29 ± 0.04 mb.

In both exit channels, the peaks in the spectra are seen to occur at similar mutual excitation energies for each of the three entrance channels. For low excitation energies, where the density of possible mutual excitations is small, this similarity between spectra is expected. At higher energies, where the level density increases, the common peak structure becomes significant and indicates that the mechanism which produces these peaks is not entrance-channel dependent.

D. Particle-particle-γ measurement for ^{12}C(^{36}Ar,^{24}Mg)^{24}Mg

To explore the origin of the peaks observed at higher excitation energies in the ^{20}Ne + ^{28}Si and ^{24}Mg + ^{24}Mg exit-channel spectra, γ-ray data taken in coincidence with the particle-particle coincidence yields for the ^{36}Ar + ^{12}C reaction were analyzed, focusing on the contributions of the ^{24}Mg ground-state rotational band.

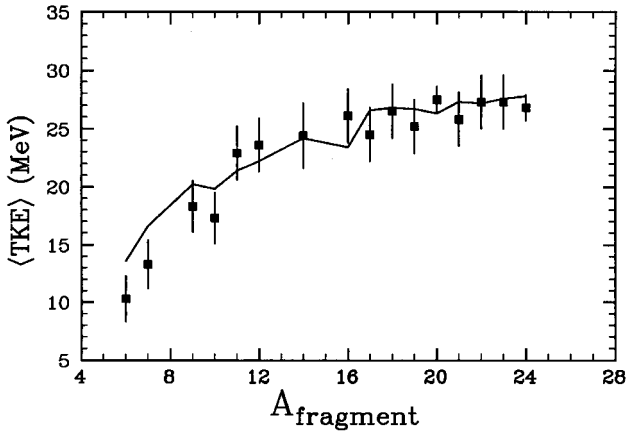

FIG. 5. Observed and calculated average c.m. total kinetic energies. The symbols represent the data and the line connects values obtained from the model calculation.

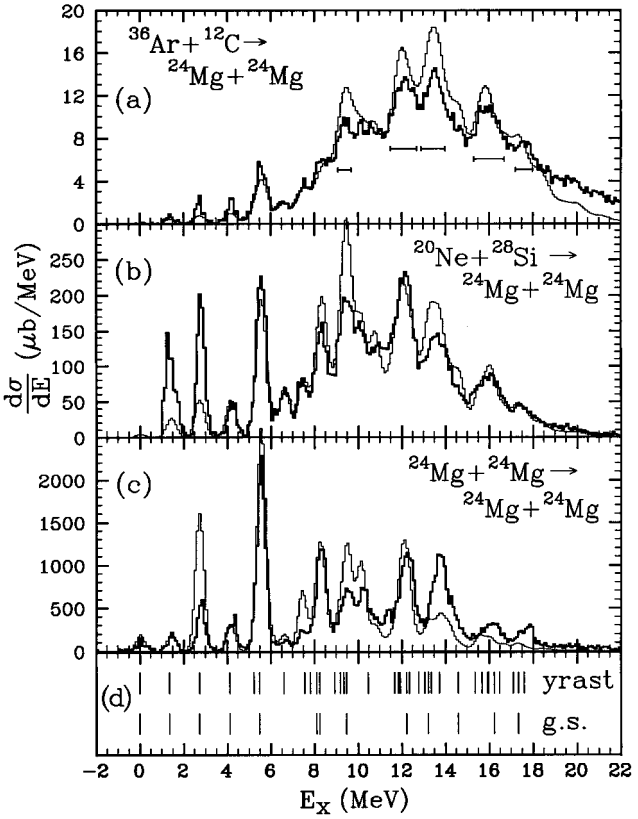

FIG. 6. The ^{24}Mg + ^{24}Mg mutual-excitation spectra for the three different entrance channels. Spectra derived from experiment are indicated by the thick-line histograms. Spectra obtained from the model calculation are indicated by the thin-line histograms and for each channel have been scaled by the ratio of experimental to calculated cross section. The five horizontal bars in (a) mark the energy ranges used in the γ-ray analysis. The vertical lines in (d) mark the mutual excitations below 18 MeV involving the ground-state rotational band and all yrast states.

The Doppler-corrected γ-ray spectra for the ^{28}Si(^{20}Ne,^{24}Mg)^{24}Mg and ^{12}C(^{36}Ar,^{24}Mg)^{24}Mg reactions gated on excitation energy from 7.5 MeV to 18 MeV are shown in Fig. 8. The spectra are plotted with a logarithmic energy scale so that the Doppler broadening of peaks appears constant [2]. Since it is not possible to know which of the two reaction fragments a given γ ray originates from, each γ ray is corrected for both possible Doppler shifts, with two different energy bins in the histogram incremented for a given event. To avoid the phantom structures that can result from this procedure when there is a strong transition, the complementary Doppler corrections were suppressed for the dominant $2_1^+ \rightarrow$ g.s. and $4_1^+ \rightarrow 2_1^+$ transitions. Within the limits imposed by the statistics, the experimental spectra appear to be similar, although with possible differences in the yields for specific transitions. A statistical model calculation that appears to be in qualitative agreement with these results is presented in Sec. IV B. The intrinsic resolution of the Ge detectors was found to be $\simeq$ 0.1%, although Doppler broadening limited the observed resolution to $\simeq$ 0.5%.

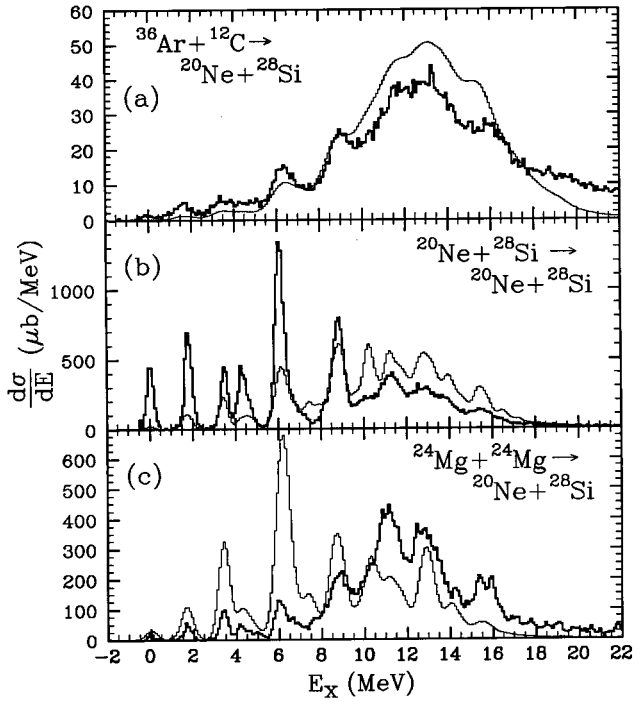

FIG. 7. The ^{20}Ne + ^{28}Si mutual-excitation spectra for the three different entrance channels. Spectra derived from experiment are indicated by the thick-line histograms. Spectra obtained from the model calculation are indicated by the thin-line histograms and for each channel have been scaled by the ratio of experimental to calculated cross sections.

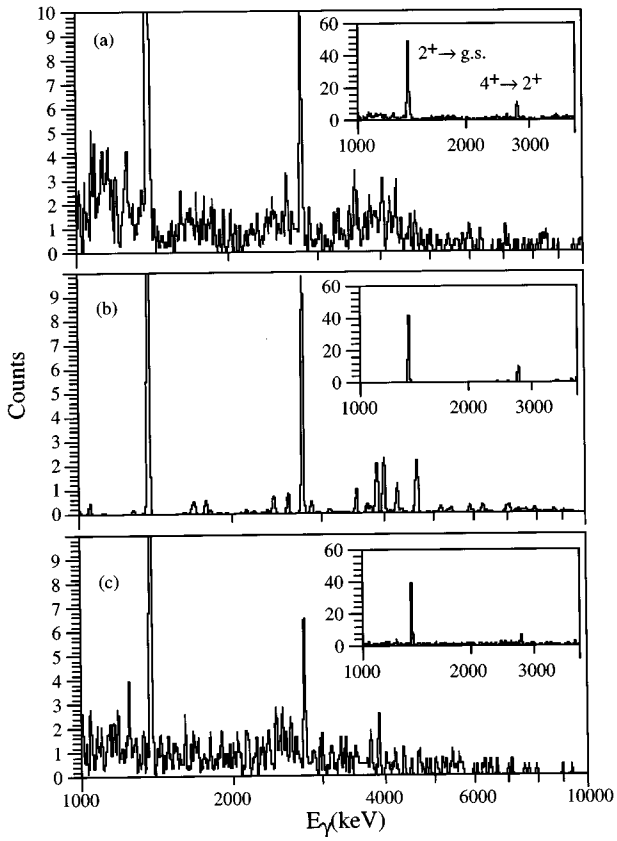

FIG. 8. (a) Experimental and (b) model-calculated γ-ray spectra for the ^{12}C(^{36}Ar,^{24}Mg)^{24}Mg reaction. (c) Experimental spectrum for the ^{28}Si(^{20}Ne,^{24}Mg)^{24}Mg reaction. All three spectra correspond to range in excitation energy of 7.5–18.0 MeV. The insets allow a comparison of the low-lying transitions that are otherwise off scale.

To examine whether the peaks at higher energies in the excitations-energy spectra result from ''special'' structure in the compound system leading to the enhanced populations of specific mutual excitations, such as, for example, the selective population of mutual yrast excitations, the γ-ray data were gated on the five excitation-energy ranges indicated in Fig. 6(a) and closely inspected for evidence of yrast transitions. Although the counting statistics were low, the good intrinsic energy resolution of the Ge detectors and the known γ-ray intensities made it possible to positively identify several transitions and to infer the absence of others. If structures in the excitation-energy spectra are in fact based on mutual excitations of levels in the ground-state rotational band of ^{24}Mg or yrast levels, in general, then one expects to see some specific relative strengths among associated γ-ray transitions. A detailed analysis was made of the data for each of the five energy ranges (see Ref. [15] for details), and it was found that for the entrance channel considered here, the high-lying peaks in the ^{24}Mg + ^{24}Mg mutual-excitation spectrum at these energies are not dominated by simple excitations exclusively involving levels in the ground-state (g.s.) rotational band.

IV. DISCUSSION

A. Fission model description of mass and total kinetic energy distributions

Over the past few years it has been shown that the fission process in light nuclear systems can be successfully described using the same transition-state formalism that has become the standard description of fission in heavier systems. This model assumes the formation of a fully equilibrated compound nucleus that subsequently breaks apart into two fragments. The probability of the breakup to a given mass channel is governed by the phase space available at the most restricted point in the breakup process, the so-called ''transition point.'' Since the free energy in the fissioning system has its minimum value at the saddle point of the macroscopic energy surface, this is usually taken as the transition point.

Assuming spinless particles in the entrance channel, the cross section for a reaction with entrance channel α and exit channel β can be expressed using the Hauser-Feshbach formalism with

$$\sigma_{\alpha\beta}=\sum_J \sigma_J(\alpha)\frac{\Gamma_J(\beta)}{\sum_\lambda \Gamma_J(\lambda)}, \tag{1}$$

where $\sigma_J(\alpha)$ is the partial cross section for forming the compound nucleus with spin J, $\Gamma_J(\beta)$ is the decay width to channel β, and λ is an index that ranges over all possible decay channels. The decay channels are usually grouped in terms of γ-emission, light-particle evaporation and fission channels. Schematically, the total decay width can be expressed as

$$\sum_{\lambda} \Gamma_J(\lambda) = \Gamma_J^{\gamma} + \Gamma_J^{ER} + \Gamma_J^{fis}, \quad (2)$$

where Γ_J^{γ}, Γ_J^{ER}, and Γ_J^{fis} are the sum of the decay widths for the respective processes at a compound-nucleus spin J. The particle widths can be expressed in terms of transmission probabilities $T_J(\lambda)$ and the compound-nucleus level density ρ_{CN}, with

$$\Gamma_J(\lambda) = \frac{T_J(\lambda)}{2\pi\rho_{CN}(E^*_{CN}, J)}. \quad (3)$$

Fission usually occurs early in the decay chain of the compound system, where the γ-decay width is small compared to the particle branches. For the evaporation channels, the transmission probabilities are found by optical-model calculations and the sum over channels can be expressed as an integral over the energy-dependent level densities in the residual nuclei. For fission, the transmission probabilities are taken as unity for energetically allowed paths and zero otherwise. Here, the number of channels is then assumed to be given by the level density above the saddle-point configuration (i.e., the transition state). In light systems, the spin and mass asymmetry dependence of the saddle-point energy must be explicitly considered. Effects resulting from the finite range of the nuclear interaction and the diffuseness of the nuclear surface also have an important influence on the macroscopic energies calculated for these systems. Explicit expressions for the appropriate fission widths for lighter systems can be found in Ref. [1] and are based on the Sierk fission barriers.

Saddle-point configurations in light systems are believed to have the shape of two touching spheroids separated by a relatively narrow neck region. As the system passes over the saddle point, towards greater deformation of the compound system, the neck eventually breaks at the scission point. Although there can be additional energy damping as the system progresses from the saddle to scission configurations, the energy difference between these two shapes is expected to be small in low-mass systems. Consequently, the total kinetic energy of the final fragments can be related to the sum of the relative nuclear, Coulomb, and rotational energies of the two spheroids which comprise the saddle-point shape. The relative radial velocity of the two fragments at the saddle point can lead to an additional kinetic energy component for the final fragments, but the weighting of the fission decay widths by the saddle-point phase space leads to a preferential decay to channels where this latter energy is small.

The fission mass distribution obtained from the transition-state calculations is compared to the experimental results for the ^{36}Ar + ^{12}C reaction in Fig. 4. For this comparison, the fission model predictions have been corrected for secondary light-particle emission using the code LILITA [16]. (Second-chance fission from the reaction fragments is expected to occur at $\ll 1\%$ of the secondary light-particle emission rate.) The calculated values for the total kinetic energy of the fragments $\langle E_{TKE} \rangle$, after correcting for the influence of secondary light-particle evaporation, are shown in Fig. 5. The same parameter values are used in the calculations as have been found to successfully describe the fission yields for the ^{24}Mg + ^{24}Mg reaction [7] and, more generally, have been found to result in a global description of the fission process in light systems [1]. A Wigner-energy correction is applied to the saddle-point energies to achieve the preferential population of the $4n$ nuclei, as seen experimentally [1]. The agreement between experiment and the results of the model calculations is quite good, especially when one considers the macroscopic nature of the model. In order to achieve the agreement between the model calculation and experiment seen in Figs. 4 and 5, it was necessary to assume a total fusion cross section of 1000 mb, resulting in a calculated ER cross section of 970 mb. This value is at the low end of the experimental limit given in Sec. III A. The most significant disagreement between the model calculation and the ^{36}Ar + ^{12}C results occurs for the calculated mass asymmetry, which is less than that indicated by the data. This is in contrast to the earlier analysis [7] of the ^{24}Mg + ^{24}Mg reaction where good agreement between the calculated and experimental results was achieved. The discrepancy in the ^{36}Ar + ^{12}C results may be a consequence of an additional deep-inelastic, orbiting contribution associated with the entrance-channel mass partition. A similar result has been observed in the ^{47}V compound system which has been studied with the near-symmetric ^{23}Na + ^{24}Mg and asymmetric ^{35}Cl + ^{12}C entrance channels [17,18]. There, the model calculation was found to be in agreement with the results from the near-symmetric measurement. However, for the asymmetric entrance channel leading to the same compound-nucleus excitation energy, the calculation predicted a less mass-asymmetric distribution than observed and overpredicted the observed fission cross sections unless a relatively low fusion cross section was assumed.

B. Excitation-energy spectra

It has been shown for the ^{32}S + ^{24}Mg [2] and ^{24}Mg + ^{24}Mg [7] reactions that much of the structure seen at higher energies in the excitation-energy spectra can be understood in terms of the statistical population of levels in the fragments. In these cases, the model calculation used to describe the experimental results was based on an extension of the ideas of the Hauser-Feshbach and transition-state pictures.

In order to describe the structure observed in excitation energy spectra it is necessary to predict how specific mutual excitations will be populated in the fission fragments. This is feasible in the light systems being studied since the energy levels of the final fragments are known to relatively high energies from γ-ray spectroscopy and α-particle scattering studies. Unfortunately, the standard transition-state picture follows the decay of the compound nucleus to the saddle point, but says little about the subsequent stages of the decay process. In particular, the model fails to account for the population of specific mutual excitations in the fragments. An alternative description of the binary breakup in terms of an ''extended Hauser-Feshbach'' method treats the fission channels of Eq. (1) in a manner analogous to the light-particle evaporation channels [19], thereby allowing for the fragment levels to be explicitly incorporated in the calculations. It is still not clear, however, how to calculate the transmission probabilities for the fission channels within this formalism. These probabilities should, presumably, reflect the macroscopic energy surface underlying the decay path from the compound nucleus to the final fragments. Although the

extended Hauser-Feshbach model is still under development [20], at present *ad hoc* transmission probabilities are used that are based on the experimental fission systematics. *Ab initio* calculations based on the macroscopic energy surface have not yet been developed, although sufficient systematics have been established to allow for reasonable predictions based on this model.

In order to retain the system independence of the transition-state calculations, where realistic saddle-point shapes and energies are explicitly incorporated into the fission decay widths, a procedure has been developed to calculate the population of specific mutual excitations in the fragments based on the level densities at the saddle point. The assumption is made that a thermal distribution of states is maintained at the saddle point and that these states decay with statistical weightings to the final fragment excitations. Within the transition-state method, the saddle-point levels already correspond to a commitment to fission into a particular mass partition. The transmission probabilities are therefore taken as unity, independent of the particular fragment states populated. The cross section for populating a specific mutual excitation (β_1,β_2) is then given by

$$\sigma(\beta_1,\beta_2)=\sum_J \sigma_{\rm ff}(J,\eta)\frac{\sum_{\ell_{\rm out}}[\beta_1\times\beta_2]_{J,\ell_{\rm out}}P(\eta,J,\epsilon)}{\sum_{\lambda_1,\lambda_2,\ell_{\rm out}}[\lambda_1\times\lambda_2]_{J,\ell_{\rm out}}P(\eta,J,\epsilon)}, \tag{4}$$

where $\sigma_{\rm ff}(J,\eta)$ is the partial cross section for producing the compound nucleus at spin J that subsequently fissions into a mass partition η, $[\lambda_1\times\lambda_2]_{J,\ell_{\rm out}}$ represents the sum of the possible spin couplings between the two fragments in states λ_1 and λ_2 with orbital angular momentum $\ell_{\rm out}$ and coupling to compound-nucleus spin J, and $P(\eta,J,\epsilon)$ is the probability of the compound nucleus of spin J to fission with mass asymmetry η and radial kinetic energy ϵ. It should be noted that $P(\eta,J,\epsilon)$ depends implicitly on $\ell_{\rm out}$ through ϵ.

The radial kinetic energy ϵ can be expressed in terms of the characteristic energies of the reaction with

$$\epsilon=E_{\rm c.m.}+Q_0-V_{\rm rel}(\ell_{\rm out},\eta)+\delta-E_x\,. \tag{5}$$

Here, $E_{\rm c.m.}$ is the center-of-mass energy in the entrance channel, Q_0 is the ground-state Q value, $V_{\rm rel}(\ell_{\rm out},\eta)$ is the relative energy of the two spheroids that comprise the saddle-point shape, δ is the energy loss that occurs in moving from the saddle to scission configurations, and E_x is the mutual excitation of the final fragments. For the present work, δ is taken equal to zero, consistent with the saddle and scission configurations being similar. Further details of the calculation can be found in Ref. [2].

The results of this calculation are shown by the thin-line spectra in Figs. 6 and 7. The spin weighting was determined with the known level schemes for ^{20}Ne [21], ^{24}Mg, and ^{28}Si [22–28]. For comparison with experiment, the calculated spectra were generated by assuming Gaussian line shapes for the discrete excitations, with the Gaussian width set to be consistent with the experimental resolution. Although both particle unbound and bound states were included in the calculations, the calculated spectra shown in the figures correspond to particle-bound states only. This is appropriate since the experimental data was required to satisfy a coplanarity condition that discriminates against events involving secondary particle emission.

The calculation successfully reproduces the positions of the peaks seen in the experimental spectra. In order to emphasize differences in relative magnitudes of the peak cross sections, the calculated spectra have been normalized to the energy-integrated experimental cross sections. The relative cross sections in each of the peaks are reproduced fairly well, with most of the large discrepancies occurring for low excitation energies. The ^{24}Mg(^{24}Mg,^{24}Mg)^{24}Mg reaction has a known resonance component near the beam energy. Although such behavior cannot be accounted for by this purely statistical model, it is clear that the model can account qualitatively for the peak structure at high excitation energies as well as for most of the cross section going to this structure. The overall agreement between the calculated and observed spectra, and the appearance of essentially the same structure in both exit channels for all three entrance channels, supports the conclusion that most of the structure and yields seen in these mutual-excitation spectra can be understood in terms of statistical fission from a compound nucleus.

Figure 8 shows the experimental and calculated γ-ray spectra for the ^{12}C(^{36}Ar,^{24}Mg)^{24}Mg reaction gated on excitation energy from 7.5 MeV to 18 MeV. As with the excitation spectra, the model calculation is in good agreement with the experimental results. Also shown is the corresponding experimental spectrum obtained with the ^{28}Si(^{20}Ne,^{24}Mg)^{24}Mg reaction. In each case a Gaussian smoothing function has been applied to facilitate the comparison of the low-statistics spectra. The width of the peaks in the calculated spectrum is set comparable to that of the experimental results to aid in comparing these spectra. The calculated spectrum is also based on the same energy-integrated particle yield as found experimentally.

The insets in Fig. 8 show that the ratio of the $4_1^+\rightarrow 2_1^+$ and $2_1^+\rightarrow$g.s. transitions is well reproduced by the calculations, indicating that the calculation correctly accounts for the fraction of the yield that goes into high-spin states of the fragments (which decay predominantly through the 4^+ level). Closer inspection of the details of the experimental and calculated spectra also indicates that the general behavior is reproduced, although significant differences between the calculated and observed yields for specific transitions are observed. An exploration of these differences will require measurements with better statistics.

C. Deduction of fission partial cross section distribution

Although the model calculation is in good agreement overall with the experimental excitation-energy spectra obtained from the particle data, there are significant discrepancies in the relative yields for a few specific peaks. We can group the possible reasons for these discrepancies into three categories. The first category can be described as incorrect input to the model and includes several possibilities. The partial cross section distribution used for fusion can affect the calculated results, yet is poorly determined. Also, the incorrect assignment of the spin of a state or incorrect branching ratios for a state used in the calculation can have a

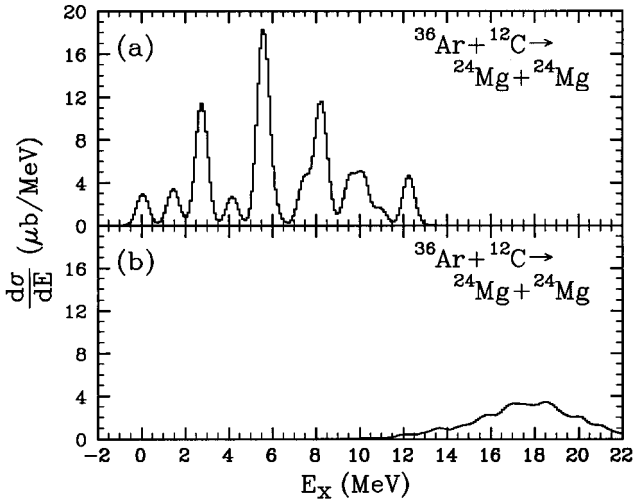

FIG. 9. Mutual-excitation spectra for particle-bound states, calculated by assuming a 50 μb partial cross section at compound-nucleus spins of (a) $32\hbar$ and (b) $16\hbar$.

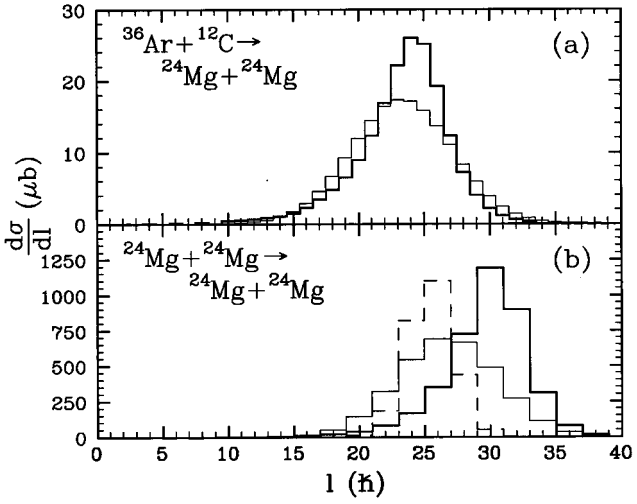

FIG. 10. Calculated (thick-line) and fitted (thin-line) fission spin distributions for the (a) ^{12}C(^{36}Ar,^{24}Mg)^{24}Mg and (b) ^{24}Mg(^{24}Mg, ^{24}Mg)^{24}Mg reactions. In (b) the thin-line histogram results from the fit to the experimental excitation spectrum, and the dotted histogram results from the fit to the estimated nonresonant excitation spectrum.

significant influence on the calculated mutual-excitation spectra. Here, uncertainties in the available level structure data are a primary limitation. The second category includes second-order details not included in the model itself. These might consist of, for example, effects of the microscopic structure of the compound system on the fission barriers. In the third category we include yields from all processes which the model, by design, does not describe. This includes all mechanisms which do not proceed through statistical fission of a compound nucleus and statistical population of fragment excited states.

Imperfections in the model calculation as a result of the limitations found in the fusion spin distribution or fission barriers would affect, among other things, the calculated fission spin distribution $\sigma_{\rm ff}(J,\eta)$. Although relatively small, the disagreements between the observed and calculated fission cross sections for individual mass channels suggest that such imperfections are significant.

To explore this possibility, we fitted the calculated spectra to the corresponding experimental spectra by varying the assumed fission spin distribution. This analysis was done by parametrizing the spin distribution and then doing a least squares fit of the calculated spectrum to the experimental spectrum, adjusting this distribution. The experimental spectra were fitted over the full range of excitation energy for which events involving secondary evaporation could be ignored. This limited the fitting region to maximum excitation energies of 18 MeV for the ^{36}Ar + ^{12}C entrance channel and 17 MeV, 20 MeV, 17 MeV, and 19 MeV, respectively, for the asymmetric and symmetric exit channels of the ^{20}Ne + ^{28}Si and ^{24}Mg + ^{24}Mg entrance channels. Each spin contributes to a large range of excitation energies, as shown in Fig. 9 where excitation spectra calculated for compound-nucleus spins of $32\hbar$ and $16\hbar$, respectively, are displayed. The constraints afforded by the experimental data were not sufficient to obtain unique descriptions of the complete fission spin distribution and several functions were found to give equally good fits to the excitation spectra. A parametrization based on a Gaussian shape was adopted because of its simple form and minimal number of parameters. Examples of calculated and fitted fission spin distributions are shown for the ^{12}C(^{36}Ar,^{24}Mg)^{24}Mg and ^{24}Mg(^{24}Mg,^{24}Mg)^{24}Mg reactions in Fig. 10. The shape of these distributions is representative of all of those which we have examined.

The resulting fitted spectra (thin line) are shown, along with the experimental spectra (thick line) in Figs. 11 and 12. The mean and standard deviations for each of the corresponding fission spin distributions are given in Table II. Although these moments are obtained from the Gaussian fit, other functional forms for the distribution were found to result in similar values. Based on the dependence of χ^2 on changes in $\langle l \rangle$ we estimate the precision of $\langle l \rangle$ obtained from the fitting procedure to be approximately $(1–1.5)\hbar$. Considering the simplicity of the model, the fitted spectra do a remarkably good job of reproducing the experimental spectra. In the following discussion we focus on the discrepancies and some of their possible sources.

1. ^{24}Mg + ^{24}Mg exit channel

Of the three entrance channels examined, the model best reproduces the mutual-excitation spectra obtained with the ^{36}Ar + ^{12}C entrance channel. In this case [see Fig. 6(a)] there is only a slight excess in the four peaks seen between 9.0 and 16.5 MeV. The fitted spectrum [Fig. 11(a)] is in excellent agreement with experiment, showing only a small excess yield in the 9.5 MeV peak.

For the ^{20}Ne + ^{28}Si entrance channel, the largest differences occur in both the calculated [Fig. 6(b)] and fitted spectra [Fig. 11(b)] at the 1.4 and 2.7 MeV peaks. These peaks correspond, respectively, to the $0^+_1 + 2^+_1$ and $2^+_1 + 2^+_1$ mutual excitations. The fit shows a small excess yield for the peak near 13.5 MeV and a small deficiency in yield for the peak near 12 MeV. For each of these two peaks, the fitted spectrum is not dominated by any single mutual excitation. Also, in each case the specific levels involved in the three excita-

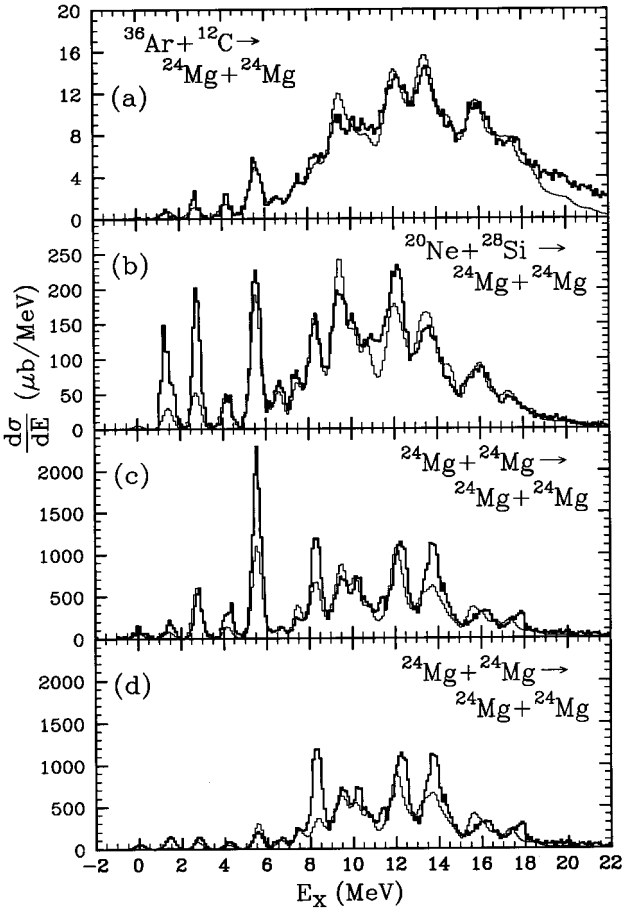

FIG. 11. (a)–(c) Fitted (thin-line histograms) and experimental (thick-line histograms) ^{24}Mg + ^{24}Mg mutual-excitation spectra for the three different entrance channels. (d) Same as (c) except that below 6.2 MeV the spectrum (thick line) is an estimate of the nonresonant contribution. The fit to this spectrum is shown as the thin-line histogram.

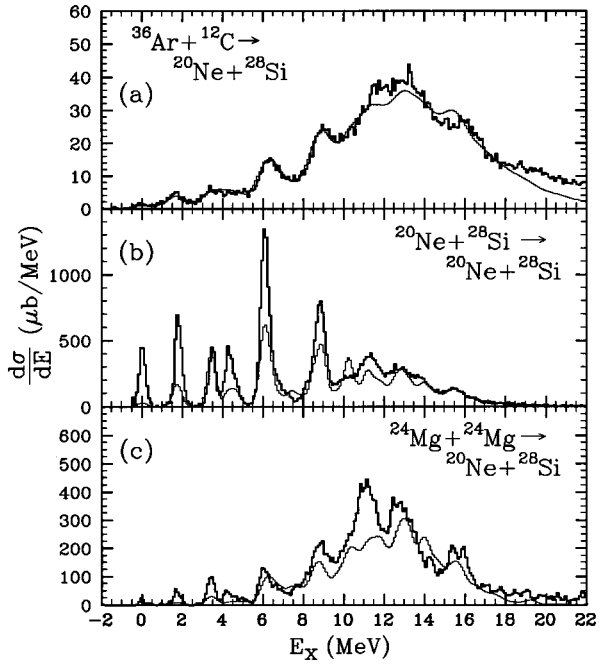

FIG. 12. Fitted (thin-line histograms) and experimental (thick-line histograms) ^{20}Ne + ^{28}Si mutual-excitation spectra for the three different entrance channels.

tions with the largest cross sections have well-established spin assignments.

The ^{24}Mg + ^{24}Mg entrance channel has its largest discrepancies between the fitted [Fig. 11(c)] and experimental spectrum at peaks near 4, 5.5, 8.3, and 13.5 MeV. Both the fitted and calculated spectra underpredict the yield in the peak near 13.5 MeV. Again, this peak is not dominated by a single mutual excitation in the calculation. Unlike the other two entrance channels studied, where there was no significant difference in calculated and fitted fission spin distributions, for this entrance channel the distribution obtained from the fit had a mean value $3\hbar$ less than that obtained from the calculation (see Table II). The ^{24}Mg(^{24}Mg,^{24}Mg)^{24}Mg reaction is known [3–5] to involve a nonstatistical, resonance mechanism which contributes to yields at lower mutual-excitation energies. Since the model cannot account for such effects, the excitation-function data shown in Fig. 1 of Ref. [3] was used to obtain an estimate for the nonresonant contribution to peaks below 6.2 MeV, assuming that the fission and resonance mechanisms occur on sufficiently different time scales so that the interference is incoherent. Figure 11(d) shows the spectrum obtained using this estimate and the corresponding fitted spectrum. If the resonance and statistical-fission processes interfere coherently, somewhat larger nonresonant yields might be indicated. The resulting fission spin distribution, obtained by fitting the resonance subtracted spectrum and shown by the dashed line in Fig. 10(b), has $\langle l \rangle = 25\hbar$ with a standard deviation of $1.8\hbar$. This amounts to a considerably smaller value for the mean of the spin distribution, as compared to the calculated value of $30\hbar$. The result is particularly significant since there is good agreement between the fitted and calculated distributions obtained for the two asymmetric entrance channels.

Competition between the resonance and fission processes provides the most likely explanation for the observed fission spin distribution. The resonance configuration can be envisioned as a simple ''doorway'' state through which flux passes in going between the compound nucleus and asymptotic binary channels. In general, this state can be a feature of either the entrance or the exit channel [29]. Also, a doorway state can be classified as being either ''strong'' or ''weak,'' depending on how much of the flux corresponding to a given partial wave passes through it. The success of the transition-state method in describing the main features of the ^{24}Mg + ^{24}Mg fission yields, using the same parameters as also found appropriate for the ^{20}Ne + ^{28}Si and ^{36}Ar + ^{12}C entrance channel, suggests that a strong entrance-channel doorway configuration is unlikely. Such a configuration, if it existed, would be expected to have a strong influence on the compound-nucleus spin distribution leading to fission and, therefore, would affect almost all of the fission-channel observables. An exit-channel doorway in the near-symmetric-mass breakup channels of the compound nucleus would explain the experimental observations. In this scenario, the higher-spin states of the compound nucleus that would normally contribute to the symmetric fission channel are directed into the resonance mechanism, reducing the contribu-

TABLE II. Mean and standard deviations for each of the fission spin distributions obtained with the model calculation and fits to the experimental mutual-excitation spectra.

Reaction	$\langle l \rangle_{calc}$ ($\hbar$)	$\sigma(l_{calc})$ ($\hbar$)	$\langle l \rangle_{fit}$ ($\hbar$)	$\sigma(l_{fit})$ ($\hbar$)
^{36}Ar + ^{12}C→^{24}Mg + ^{24}Mg	23	3.6	23	3.8
^{36}Ar + ^{12}C→^{20}Ne + ^{28}Si	23	3.6	21	5.9
^{20}Ne + ^{28}Si→^{24}Mg + ^{24}Mg	27	3.5	27	3.7
^{20}Ne + ^{28}Si→^{20}Ne + ^{28}Si	27	3.5	28	5.1
^{24}Mg + ^{24}Mg→^{24}Mg + ^{24}Mg	30	3.4	27	3.8
^{24}Mg + ^{24}Mg→^{20}Ne + ^{28}Si	29	3.4	26	2.0

tion of these partial waves to the fission spin distribution and thereby shifting the mean of this distribution to a lower value. The fission yields corresponding to the asymmetric mass entrance channels may not be as strongly influenced by the doorway configuration because the corresponding spin distributions have their maximum values at spins lower than that of the doorway state. A shell-stabilized, shape-isomeric configuration that traps the reaction flux as the system develops along the fission path might account for this behavior.

2. ^{20}Ne + ^{28}Si exit channel

As with the ^{24}Mg + ^{24}Mg exit channel, the model calculation [Fig. 7(a)] is in best agreement with experiment for the ^{36}Ar + ^{12}C entrance channel and the fitted spectrum [Fig. 12(a)] improves on this agreement. The spin distribution resulting from the fit shows a slight decrease in $\langle l \rangle$ (see Table II) from the initial calculation. This result is different from what was observed in the symmetric exit channel where no such decrease was observed. In this case (^{20}Ne + ^{28}Si exit channel) the small difference in the fitted and model calculated values of $\langle l \rangle$ may be related to an increase in ''contamination'' of the experimental bound-state spectrum at higher excitation energies by contributions from unbound states. Our discrimination against unbound states is not perfect and so reactions populating these states will increase the yields observed in the mutual-excitation spectrum at higher excitation energies. The $\langle l \rangle$ value obtained by fitting to this ''contaminated'' spectrum, where only particle-bound states are considered in the fitting procedure, will be shifted to a lower value than if the contributions from unbound states were not present.

For the ^{20}Ne + ^{28}Si entrance channel, the most significant difference between the observed spectrum and the calculated [Fig. 7(b)] and fitted [Fig. 12(b)] spectra is the deficiency in the predicted yield to peaks below 8 MeV. The peaks below and including the one near 6 MeV are dominated by mutual excitations of the 0^+_1, 2^+_1, and 4^+_1 levels in ^{20}Ne and ^{28}Si. Assuming that the model calculation is properly describing the statistical decay of the system, the excess yield relative to the model would suggest a nonstatistical origin for this low mutual excitation-energy yield. Such an origin for this yield might be associated with the resonant behavior which has been observed with the ^{20}Ne + ^{28}Si reaction [6].

The calculated spectrum for the ^{24}Mg(^{24}Mg, ^{20}Ne)^{28}Si reaction [Fig. 7(c)] only poorly reproduces the observed spectrum. The fitted spectrum [Fig. 12(c)] is more successful, although it clearly underpredicts the yield to the peak near 11 MeV. As with the ^{24}Mg(^{24}Mg, ^{24}Mg)^{24}Mg reaction, the mean of the fission spin distribution obtained from the fit is shifted down by $3\hbar$ relative to the value obtained from the calculation. Also, as with the symmetric case, this result can be interpreted in terms of competition between a resonance and a fission process for decay of the high-spin states in the compound nucleus. It is possible that the spin distribution is shifted to a lower value because the high-spin compound-nucleus configurations predominately decay through ^{24}Mg + ^{24}Mg resonance channels, although at a slightly higher excitation energy, there is evidence for such a correlation between the mass-symmetric and -asymmetric decay channels in the ^{48}Cr system [30].

V. SUMMARY AND CONCLUSIONS

The fission decay of the compound ^{48}Cr system is studied at $E^*_{CN} \approx 60$ MeV using the ^{36}Ar + ^{12}C and ^{20}Ne + ^{28}Si entrance channels. The results are compared with those from an earlier measurement using the ^{24}Mg + ^{24}Mg entrance channel. Results of a transition-state model calculation are found to be in good general agreement with the mass and total kinetic energy distributions obtained from the ^{36}Ar + ^{12}C measurement, although it was necessary to assume an evaporation-residue cross section at the low end of the experimental uncertainty.

Three results from the present study support the conclusion that the narrow structures and most of the yield observed at high excitation energy in the mutual-excitation spectra can be understood in terms of fission decay of a compound nucleus followed by the statistical population of excited states in the fission fragments. First, mutual-excitation spectra for the ^{24}Mg + ^{24}Mg and ^{20}Ne + ^{28}Si exit channels were compared for all three entrance channels and it was found that at high excitation energy, where the density of possible mutual excitations is large, similar peak structures are present for all three entrance channels. Second, particle-particle-γ coincidence data from the ^{36}Ar + ^{12}C measurement show that high-energy peaks in the ^{24}Mg + ^{24}Mg mutual-excitation spectrum are not dominated by simple excitations of levels in the ^{24}Mg ground-state rotational band. Third, spectra calculated using a statistical-model calculation are in overall good agreement with experimental spectra at high excitation energy. We cannot,

however, rule out the possibility that some part of the structure seen at high excitation energy in the ^{24}Mg(^{24}Mg, ^{24}Mg)^{24}Mg reaction is related to nonstatistical processes. Additional γ-ray studies have been planned to resolve this question.

There are some discrepancies between the observed and calculated spectra in terms of the relative yields to some specific peaks. These discrepancies may result from one or more causes, including problems with the model description of the fusion spin distribution, microscopic effects not included in the fission calculation, limitations related to the level structure data used, and the presence of nonstatistical yields. More work needs to be done to understand these effects.

Information about the fission spin distribution extracted from fits to the experimental data and from the model calculations is consistent with the interpretation that there is significant competition between the fission and resonance mechanisms for the highest-spin states of the compound nucleus. One possibility is that there exists a shape-isomeric configuration in the compound system that results in an exit-channel doorway state. As the system progresses along the fission path, it may be possible for flux to become trapped in this doorway configuration, thereby depleting the cross section, leading to symmetric-mass fission. A strong doorway configuration in the entrance channel would be expected to have a stronger overall influence on the fission behavior than is observed and is therefore deemed unlikely. Still unresolved is the question of relative time scales between the resonance and fission processes. Although the resonance lifetimes can be determined from the observed energy widths, there is relatively little experimental evidence concerning the fission lifetimes. If these two processes result from the same compound-nucleus spins, as suggested by this work, a determination of their relative time scales would help to establish the degree of coherence between them.

ACKNOWLEDGMENTS

This work was supported in part by the U.S. Department of Energy, Nuclear Physics Division, under Contracts Nos. DE-FG02-89ER40506 and W-31-109-ENG-38. Additional support for the Strasburg-Kansas Collaboration has come from an NSF International Programs Grant. Two of us (C.B. and R.M.F.) would like to acknowledge the Centre National de la Recherche Scientifique for financial support within the framework of the CNRS/NSF collaboration program.

[1] S.J. Sanders, Phys. Rev. C **44**, 2676 (1991).

[2] S.J. Sanders, A. Hasan, F.W. Prosser, B.B. Back, R.R. Betts, M.P. Carpenter, D.J. Henderson, R.V.F. Janssens, T.L. Khoo, E.F. Moore, P.R. Wilt, F.L.H. Wolfs, A.H. Wuosmaa, K.B. Beard, and Ph. Benet, Phys. Rev. C **49**, 1016 (1994).

[3] R.W. Zurmühle, P. Kutt, R.R. Betts, S. Saini, F. Haas, and O. Hansen, Phys. Lett. **129B**, 384 (1983).

[4] A.H. Wuosmaa, R.W. Zurmühle, P.H. Kutt, S.F. Pate, S. Saini, M.L. Halbert, and D.C. Hensley, Phys. Rev. Lett. **58**, 1312 (1987).

[5] A.H. Wuosmaa, R.W. Zurmühle, P.H. Kutt, S.F. Pate, S. Saini, M.L. Halbert, and D.C. Hensley, Phys. Rev. C **41**, 2666 (1990).

[6] S.P. Barrow, R.W. Zurmühle, D.R. Benton, Y. Miao, Q. Li, P.H. Kutt, Z. Liu, C. Lee, N.G. Wimer, and J.T. Murgatroyd, Phys. Rev. C **52**, 3088 (1995).

[7] A.T. Hasan, S.J. Sanders, K.A. Farrar, F.W. Prosser, B.B. Back, R.R. Betts, M. Freer, D.J. Henderson, R.V.F. Janssens, and A.H. Wuosmaa, Phys. Rev. C **49**, 1031 (1994).

[8] R.V.F. Janssens, T.L. Khoo, E. Funk, U. Garg, J. Kolata, and J. Mihelich, ''A Proposal for a BGO Sum-Energy/Multiplicity Spectrometer and Multi-Compton Suppression Spectrometer System,'' Argonne National Laboratory report, 1983.

[9] K.A. Farrar, A.T. Hasan, F.W. Prosser, S.J. Sanders, and D.J. Henderson, Nucl. Instrum. Methods A **346**, 177 (1994).

[10] F.L.H. Wolfs, Phys. Rev. C **36**, 1379 (1987).

[11] G.F. Knoll, *Radiation Detection and Measurement*, 2nd ed. (Wiley, New York, 1989).

[12] L.A. McNelles and J.L. Campbell, Nucl. Instrum. Methods **109**, 241 (1973).

[13] PACE is a modification of the program JULIAN and is described by A. Gavron, Phys. Rev. C **21**, 230 (1980). We are using a version modified by Jim Bene of Oak Ridge National Laboratory.

[14] S.J. Sanders, D.G. Kovar, B.B. Back, C. Beck, D.J. Henderson, R.V.F. Janssens, T.F. Wang, and B.D. Wilkins, Phys. Rev. C **40**, 2091 (1989).

[15] K.A. Farrar, Ph.D. thesis, University of Kansas, 1994.

[16] J. Gomez Del Campo and R.G. Stokstad, Oak Ridge National Laboratory Technical Memo No. ORNL-TM-7295, 1981 (unpublished).

[17] C. Beck, B. Djerroud, F. Haas, R.M. Freeman, A. Hachem, B. Heusch, A. Morsad, M. Vuillet-A-Cilles, and S.J. Sanders, Phys. Rev. C **47**, 2093 (1993).

[18] C. Beck, B. Djerroud, F. Haas, R.M. Freeman, A. Hachem, B. Heusch, A. Morsad, M. Youlal, Y. Abe, A. Dayras, J.P. Wieleczko, B.T. Matsuse, and S.M. Lee, Z. Phys. A **343**, 309 (1992).

[19] S.M. Lee, W. Yokota, and T. Matsuse, in ''Proceedings of the Symposium on Many Facets of Heavy-Ion Fusion Reactions,'' edited by W. Henning, D. Kovar, S. Landowne, and S. Pieper, Report No. ANL, 1986, p. 63.

[20] T. Matsuse, S. M. Lee, and C. Beck, in *Proceedings of the Symposium on Heavy-Ion Physics and its Application*, Lanzhoo 1990, edited by W.Q. Shen, X.Y. Luo, and J.Y. Liu (World Scientific, Singapore, 1991), p. 95; T. Matsuse, S. M. Lee, Y. H. Pu, K. Y. Nakagawa, C. Beck, and T. Nakagawa, in *Towards a Unified Picture of Nuclear Dynamics*, edited by Y. Abe, S .M. Lee, and F. Sakata, AIP Conf. Proc. No. 250 (AIP, New York, 1992).

[21] F. Ajzenberg-Selove, Nucl. Phys. **A475**, 1 (1987).

[22] P.M. Endt, Nucl. Phys. **A521**, 1 (1990).

[23] D. Branford, N. Gardner, and I.F. Wright, Phys. Lett. **36B**, 456 (1971).

[24] L.K. Fifield, R.W. Zurmühle, and D. P. Balamuth, Phys. Rev. C **8**, 2217 (1973).

[25] D. Branford, A.C. McGough, and I.F. Wright, Nucl. Phys. **A241**, 349 (1975).
[26] L.K. Fifield, M.J. Hurst, T.J.M. Symons, F. Watt, and K.W. Allen, Phys. Lett. **69B**, 45 (1977).
[27] S.A. Wender, C.R. Gould, D.R. Tilley, D.G. Rickel, and R.W. Zurmühle, Phys. Rev. C **17**, 1365 (1978).
[28] L.K. Fifield, E.F. Garman, M.J. Hurst, T.J.M. Symons, F. Watt, C.H. Zimmerman, and K.W. Allen, Nucl. Phys. **A322**, 1 (1979).
[29] H. Feshbach, *Theoretical Nuclear Physics: Nuclear Reactions* (Wiley, New York, 1992).
[30] S. Saini, R.R. Betts, R.W. Zurmühle, P. Kutt, and B.K. Dichter, Phys. Lett. B **185**, 316 (1987).